

Aeromechanical Response of a Distortion-Tolerant Boundary Layer Ingesting Fan

Andrew J. Provenza

NASA Glenn Research Center,
Cleveland, OH 44135
e-mail: provenza@nasa.gov

Kirsten P. Duffy

Department of Mechanical, Industrial,
and Manufacturing Engineering,
University of Toledo,
Toledo, OH 43606

Milind A. Bakhle

NASA Glenn Research Center,
Cleveland, OH 44135

Boundary layer ingestion (BLI) is a propulsion technology being investigated at NASA by the Advanced Aircraft Transportation Technology (AATT) Program to facilitate a substantial reduction in aircraft fuel burn. In an attempt to experimentally demonstrate an increase in the propulsive efficiency of a BLI engine, a first-of-its-kind subscale high-bypass ratio 22" titanium fan, designed to structurally withstand significant unsteady pressure loading caused by a heavily distorted axial air inflow, was built and then tested in the transonic section of the GRC 8' × 6' supersonic wind tunnel. The vibratory responses of a subset of fan blades were measured using strain gages placed in four different blade pressure side surface locations. Response highlights include a significant response of the blade's first resonance to engine order excitation below idle as the fan was spooled up and down. The fan fluttered at the design speed under off operating line, low flow conditions. This paper presents the blade vibration response characteristics over the operating range of the fan and compares them to predicted behaviors. It also provides an assessment of this distortion-tolerant fan's (DTF) ability to withstand the harsh dynamic BLI environment over an entire design life of billions of load cycles at design speed. [DOI: 10.1115/1.4040739]

Introduction

There are a number of computational studies which show that boundary layer ingesting propulsion systems can significantly reduce the fuel burn of an aircraft [1–6]. The potential benefits of boundary layer ingestion (BLI) (on the order of a 5–10% fuel burn reduction) are quite phenomenal because it has become increasingly more difficult to develop new ways of improving upon the performance of aircraft engines in use today. Engines that ingest an airframe boundary layer and re-energize the vehicle's wake with the thrust stream in theory show significant reductions in mission fuel burn. One of the key criterion to achieve these benefits and quite possibly the most important one is that the fan must be able to withstand the harsh unsteady loading imposed by the flow and maintain aerodynamic and aeroelastic stability while doing so. Figure 1 shows a NASA concept hybrid wing body vehicle with partially embedded boundary layer ingesting propulsors. The aft propulsors in this concept would have to be designed to handle such requirements.

A 22" subscale titanium fan, designed to structurally withstand the unsteady pressure loading caused by a heavily distorted axial air inflow, was tested in the transonic section of NASA's 8' × 6' supersonic wind tunnel. Figure 2 from Ref. [7] shows the layout of the wind tunnel model with some key features highlighted. A raised floor and a bleed system fore of the test article work to develop and vary the thickness of the boundary layer as needed for the tests. Figure 3 shows the fan slightly recessed into the floor as evident by the dipping nature of the simulated streamlines. The fan has a hub to tip ratio of 0.3 at the leading edge and the flow near the blade tip is transonic at design speed. There are 48 exit guide vanes (EGVs) with four different groups that each have different metal angles. The leading edges of the EGVs are located 5.13 inches axially aft of the fan blade trailing edges.

The unsteady pressures that this fan sees due to the distorted inflow are severe and made the design of a blade which could handle it challenging. The circumferential pressure distortion

intensity ($\Delta P_c/P$) is high: 10% at normal operating conditions. For comparison, the NASA reference S-duct inlet, "Inlet A," had a $\Delta P_c/P$ of 5.7% [8]. The BLI²DTF inlet was optimized to minimize inlet total pressure loss (ΔP_t). Reference Inlet A had a ΔP_t



Fig. 1 A NASA hybrid wing body, or blended wing body vehicle with embedded propulsors

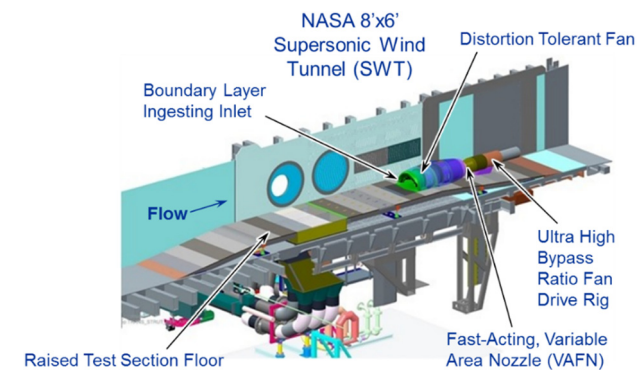


Fig. 2 Layout of the NASA GRC 8 × 6 wind tunnel test BLI²DTF fan hardware [7]

Manuscript received June 22, 2018; final manuscript received June 28, 2018; published online September 14, 2018. Editor: Jerzy T. Sawicki.

This work is in part a work of the U.S. Government. ASME disclaims all interest in the U.S. Government's contributions.



Fig. 3 Frontal view of the BLI wind tunnel model showing the ingestion of the boundary layer

of 1.8% while the ΔP_t for the BLI²DTF inlet was 0.3% [8]. The length of the inlet was reduced considerably. This reduced the total inlet pressure loss but increased the $\Delta P_c/P$. The fan was designed under contract by United Technologies Research Center for NASA. The fan has 18 Titanium Ti-6Al-4V solid blades which were designed in coupled fashion with the inlet to have sufficient structural integrity to safely survive wind tunnel testing while at the same time giving up as little typical fan stage efficiency and stability margin as possible. There were several design iterations. Details of the final design are described in Ref. [8]. The final blade design included a thicker root and a shorter tip chord as compared to the baseline blade, which was designed for podded operation on the wing in clean flow. The final blade also was restacked to balance moments around its center of gravity and to accommodate surface shot peening to reduce static stresses. A maximum fan stage efficiency of over 89% was calculated for this fan as seen in Ref. [9].

The fan successfully survived the wind tunnel testing, and visual inspection of the blades indicated that there were no surface cracks or blade damage. The vibratory responses of a subset of fan blades were measured using strain gages placed on eight of the eighteen blades in four different blade surface locations. Blade tip displacements were also measured using a noncontacting stress measurement (NSMS) system [10]. The distorted inflow total pressure profile at the aerodynamic interface plane (AIP) with the fan operating at its aerodynamic design point (ADP) for this experiment is shown in Fig. 4 [7]. This flow imposes a strong once-per-revolution and harmonic (engine order) excitation on the blades which is evident in dynamic strain data recorded from the gages. Significant resonant response of mode 1 to engine order excitation was seen below idle as the fan was spooled up and

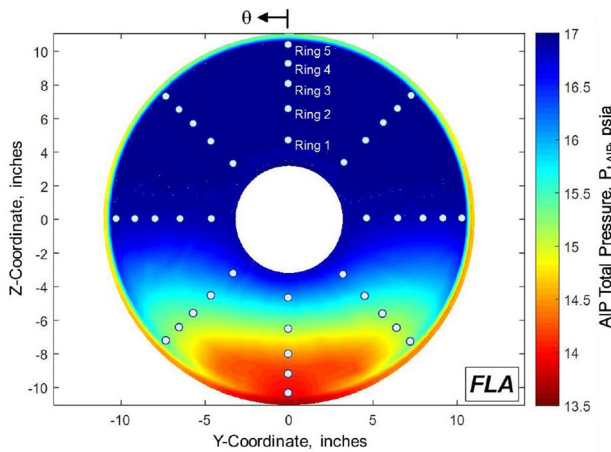


Fig. 4 Experimentally measured steady-state AIP total pressure distribution (ADP conditions) [7]

down. Flutter was also seen at the design speed under off operating line, low flow near-stall conditions. This paper presents some of the fan's vibration response characteristics. The responses are compared with some predictions of the blades' fundamental vibration modes and their expected amplitudes during operation. It also shows that this blade design met the response and fatigue life criterion established for this test.

Fan Blade Strain Measurements

Strain gages were used to capture dynamic strains on eight blades and at four surface locations. A NSMS system was used to capture the tip deflections of all the blades. Behavior of the BLI²DTF fan as measured via NSMS was presented in Ref. [10]. The gage locations and orientations were selected by UTRC using commercial mapping software and stress contour plots from finite element analysis. All gages were located on the pressure side of the blade to minimize their presence on fan performance. Figure 5 shows the four gage locations. Gages 1–3 locations were selected because they combined to provide good coverage of the first 8 blade modes. Gage 4 was added to provide duplicate coverage of mode 2 as it was predicted in Ref. [11] that for some mode 2 nodal diameter responses, the aerodynamic damping might be very low. Each blade had three gages. All eight blades had a root (leading edge) gage and two of the other three gages (trailing edge (TE), tip, or midsection). The locations of the gaged blades within the fan are shown in Fig. 6. These locations were chosen in part to distribute the gaged blades such that each quadrant had two blades. This was done to provide some local redundancy in case gages failed during testing. The blade with serial number (SN) 18 was instrumented with gages instead of the blade with SN 13 to break up the symmetry in the blade pattern. In this paper, blades are referenced by their serial number.

Table 1 lists the first 8 predicted off-resonance modal blade frequencies and nodal diameter patterns for this fan at ADP obtained using FEA. It also provides the strain ratios for each of eight modal frequencies at each of the four strain gage locations. The bold values highlighted in gray meet the usable gage ratio criterion of ≥ 0.3 . The strain ratio is equal to the gage strain divided by the absolute max principal strain for that mode. A strain ratio of 1.0 means the gage has been placed in the exact location and

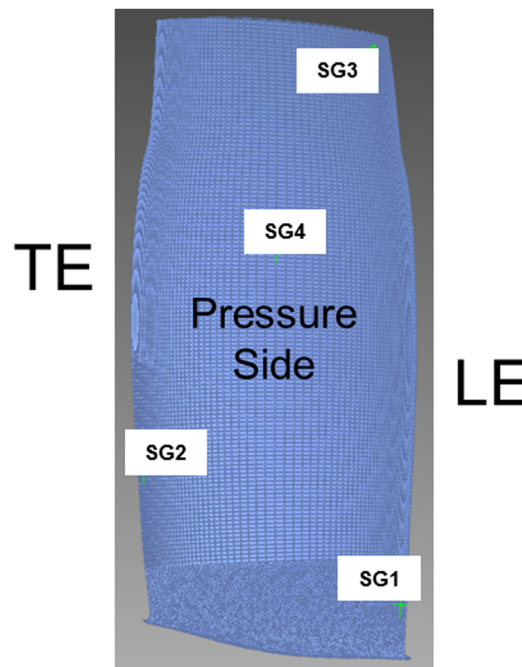


Fig. 5 Strain gage locations on titanium DTF blade

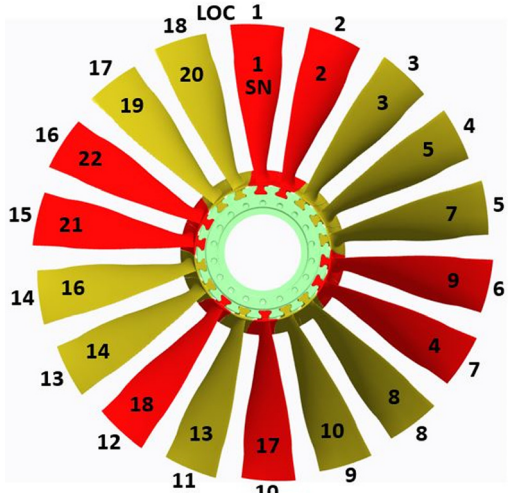


Fig. 6 Boundary layer ingestion fan wheel chart showing blade SNs and slot locations. Gaged blade SNs: 1, 2, 4, 9, 17, 18, 21, and 22.

with the exact orientation as the maximum strain in the blade when vibrating at that modal frequency. Note that the ratios for modes 1 and 2 at the SG1 location are very close to 1.0. The ratio for mode 3 at SG2 is also very high at 0.94. Since the mode 2 resonance frequency at ADP lies directly between engine orders 3 and 4, both nodal diameters 3 and 4 were analyzed. Blade modal response frequencies and patterns are sometimes a function of nodal diameter pattern [11]. In this case, however, the responses at all four gages are almost identical. In preparation for a fan test, stress limits for the first 8 modes of vibration at each of the gage locations are scaled using these ratios.

Blade Resonances

A key driver in blade design is providing adequate margin at key operating speeds between blade natural frequencies and engine order excitations. Campbell diagrams are convenient for visualizing and computing these frequency margins. Accurate predictions of the blades' fundamental vibration frequencies are required to competently determine these margins. The effect of rotation on the fundamental resonant frequencies of the final blade design was determined pretest using coupled aerostructural finite element analysis [11,12]. Mode shapes of the first four modes for relevant engine order excitations are shown in Fig. 7. Figure 8 shows the results of analysis performed both at NASA and UTRC. The experimental frequencies are also shown. By inspection, it appears that analysis predicted the frequencies and rotational effects quite well for the first four modes, then less so for the next four. Table 2 provides the percent differences between analysis

Table 1 Predicted fan blade resonant frequencies, nodal response patterns, and strain ratios for first 8 modes

Mode	Nodal diameter	Freq (Hz)	Strain ratios			
			SG1 (LE, root)	SG2 (TE)	SG3 (Tip)	SG4 (Mid)
1	1	260	0.98	0.36	0.03	0.11
2	3	697	0.99	0.12	0.29	0.70
2	4	701	0.99	0.14	0.29	0.71
3	5	1007	0.01	0.94	0.23	0.11
4	7	1413	0.59	0.62	0.67	0.52
5	9	1929	0.27	0.36	0.89	0.08
6	8	2229	0.09	0.15	0.86	0.08
7	5	2602	0.04	0.14	0.89	0.33
8	4	2865	0.06	0.09	0.83	0.02

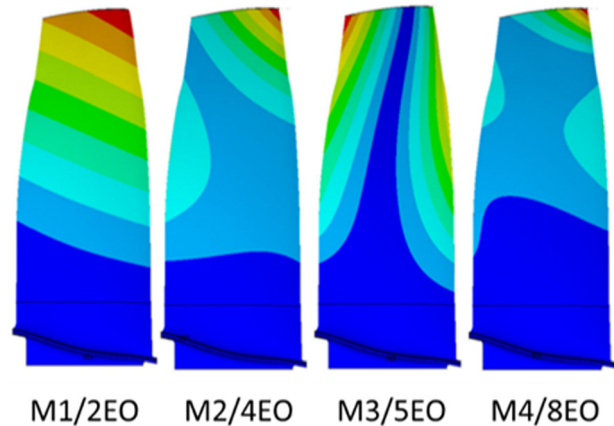


Fig. 7 First 4 blade mode shapes at relevant engine order excitations

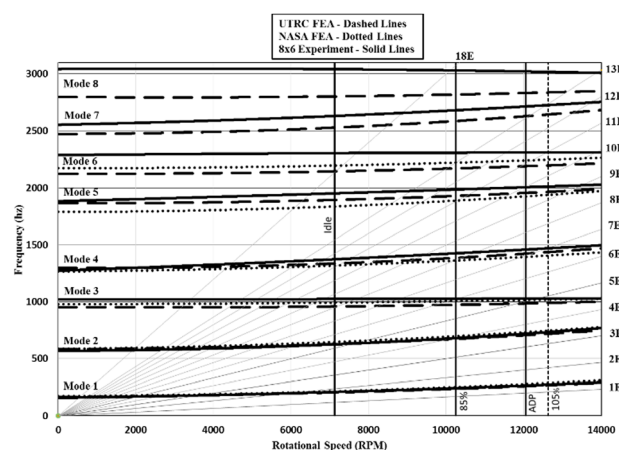


Fig. 8 BLI2DTF fan blade Campbell diagram with FEA predictions and experimental results

Table 2 Percent differences between trend line fits of FEA and experimental blade resonant frequencies versus speed data at three relevant speeds. Refer to Fig. 8.

Mode	85% Speed		100% Speed (ADP)		105% Speed	
	NASA	UTRC	NASA	UTRC	NASA	UTRC
1	3.9%	-2.4%	4.9%	-2.2%	5.2%	-2.1%
2	2.7%	-0.9%	2.0%	-1.7%	1.8%	-2.0%
3	-2.0%	-5.2%	-1.3%	-3.0%	-1.0%	-3.9%
4	-4.4%	-2.8%	-4.4%	-2.5%	-4.4%	-2.3%
5	-4.9%	-2.8%	-4.1%	-2.5%	-3.7%	-2.3%
6	-3.8%	-6.0%	-3.0%	-3.0%	-2.8%	-4.9%
7		-3.6%		-3.2%		-3.0%
8		-6.9%		-6.2%		-5.9%

and experiment at three operating speeds: 85%, 100% (ADP), and 105%. Despite the appearance that there is significantly more discrepancy between the trend lines for modes 5–8, the percent differences are similar to those from the first four modes. Mode 1–4 predictions are within $\pm 5.2\%$. Frequencies for modes 5–8 were all under-predicted but by less than 7%.

Frequency Margins

The ability of the final blade design to withstand vibration produced by the heavily distorted flow is in part affected by its frequency margins. The two most important at ADP are the M1/1EO

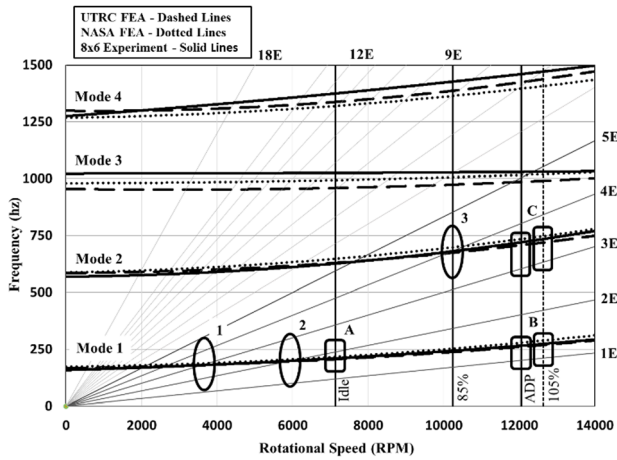


Fig. 9 BLI²DTF fan blade Campbell diagram with crossings 1, 2, 3 and frequency margins A, B, C of interest

and the M2/3EO margins. Margins of interests are identified in Fig. 9 within boxes A, B, and C. Aircraft engine fans are typically designed so that the first forward blade mode never coincides with the spin frequency (1EO) and with a minimum margin target of 10%. For the BLI²DTF fan, it was necessary to impose a similar requirement on the M2/3EO margin. These margins should also be greater than 10% at 105% speed. The reference blade M2/3EO crossing coincided with the ADP speed which proved to be problematic in terms of high cycle fatigue [8]. It remains to be determined if this frequency margin guideline used in conventional fan design needs to be increased for a distortion-tolerant fan (DTF) that operates continuously in BLI distortion. The M1/2EO margin at idle is important too because of the significant amplitude at this nearby crossing seen during start up and shutdown. Crossings of interest are identified in ellipses 1, 2, and 3 in Fig. 9. Details of crossing 2 are discussed later in this paper. Table 3 provides predicted and actual margins at idle, 85%, ADP and 105% speeds. The frequency margins from testing at A, B, and C agreed well with predictions and were more than 10%.

Blade Fatigue Life

The Goodman diagram is used to assess a blade's ability to survive dynamic stresses during a fan's operational lifetime. Blade response dynamic stress is plotted versus steady stress and an upper bound material limit curve envelopes the region where satisfactory life exists. A lifetime is represented by a number of fatigue cycles. Typically, fan blades are designed using a 10⁷ cycle lifetime curve since they typically operate in clean flow. Due to the harsh ever-present nature of this distorted flow, a 10⁹ cycle curve was used for the BLI²DTF fan. This reduces that safe life region which restricts the levels of allowable dynamic stress. If the stress conditions are such that they never combine to lie on

Table 3 Frequency margins at relevant speeds to key Campbell crossing excitations

Mode to EO	Speed	Frequency margins		
		Experiment	NASA	UTRC
M1/2EO	Idle	-13.6%	-10.1%	-15.8%
M1/1EO	ADP	24.3%	22.9%	22.6%
M1/1EO	105%	22.9%	26.8%	21.3%
M2/3EO	ADP	16.2%	17.9%	14.7%
M2/3EO	105%	13.9%	15.4%	12.1%
M2/4EO	85%	-0.5%	2.1%	-1.4%

or above the 10⁹ Goodman line, the blade could expect to have infinite life.

During the course of the BLI²DTF blade design, achieving sufficient life was challenging. The Goodman diagram in Fig. 10 shows that for the reference blade, the amplitude of the M2/3EO vibration (at ADP) could significantly exceed the limit. Two points are shown. The point closer to the line is the result of inlet shaping to reduce the effects of the distortion on the blade dynamics. Blade design changes along with inlet modifications are described in detail in Ref. [8]. Changes to the blade structure in the final design increased the mode 2 frequency near design speed which resulted in a sufficient margin of 16.2% at ADP to the 3EO excitation. The blade's dynamic stress went from a value well above the 10⁹ Goodman limit to an amplitude less than 1 ksi as seen during testing. The mode 2 dynamic stress amplitude plotted versus the steady stress at the root gage during wind tunnel testing at ADP, is also shown in Fig. 10. Changes to the blade design also reduced the steady stress at the root at ADP as is evident in the figure.

Startup Blade Response

Figure 11 shows the typical response of a blade during the startup procedure which is shown in Fig. 12. The fan was first spun up to a speed of 3200 rpm with no tunnel flow. The tunnel drives were then started and the tunnel flow was set to accelerate to 0.62 Mach. At approximately 0.32 Mach, the fan was accelerated at 125 rpm/s to 7900 rpm where it sat until the tunnel speed reached about 0.58 Mach. Two crossings are evident below 7000 rpm. At 7900 rpm, the step change in the 2EO amplitude in Fig. 11 was a result of the increase in tunnel airspeed. At about Mach 0.58, the rig was accelerated at 50 rpm/s to 11,600 rpm while the tunnel Mach was brought to 0.78. Once the air speed was close to 0.78 Mach, the rig was accelerated at 25 rpm/s to

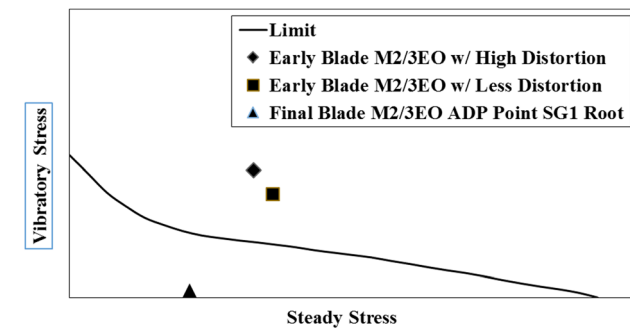


Fig. 10 Effects of inlet shape tailoring and final blade design changes on M2/3EO vibration component amplitude at SG1 root gage location at ADP

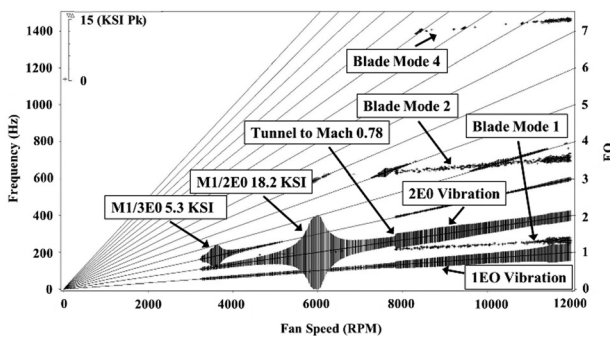


Fig. 11 Blade vibration Campbell diagram. Typical response during test rig startup at blade root.

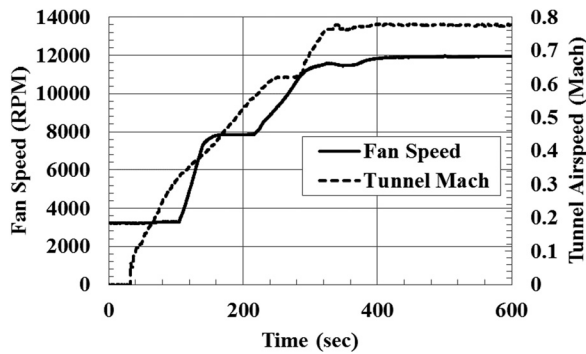


Fig. 12 Wind tunnel test rig startup air and fan speed profile

approximately 12,000 rpm. This speed varies based on tunnel conditions. The ADP is always at 11,387 rpm corrected speed.

Key Campbell Diagram Crossings

There are many speeds at which blade modes and engine order lines intersect (see Fig. 8). Three notable crossings occurred during start up and near 85% speed. These are captured by ellipses in Fig. 9 and labeled 1, 2, and 3. Response amplitudes for 1 and 2 were pointed out in Fig. 11. All three of these crossings are worth discussing. For crossing 2, amplitude is certainly of interest, but the total damping at all these crossings is important to determine and discuss.

M1/2EO Crossing Response

The largest dynamic blade response (aside from that during a brief single flutter event) was at the M1/2EO crossing. This happened at least twice during every wind tunnel test at about 6000 rpm—once during startup and once during shutdown. Occasionally, a loss of rig control would send the rig rapidly down in speed to below idle which added additional M1/2EO crossings. Table 4 presents the typical response at the root of six blades as the rig accelerated through this speed. Root gages on blades 4 and 18 were not functional when this testing occurred. Inspection of these results shows that the average amplitude of this vibration is about 16 ksi and the frequency around 199 Hz. The total damping at 2.9% is very high as compared with typical first bending mode damping values for fans operating in clean flow presented in Ref. [13]. There, typical total damping expected for this mode is said to be between 0.64% and 1.27%. This range was given for a fan bisk though it was noted that the range also applied to dove tailed blades. But even compared to the highest level of the range (1.27%), the damping measured for the BLI²DTF fan M1/2EO excursions was more than twice that. It should be noted here that in order to provide a breakdown of the total damping into structural and aerodynamic damping components (as in Table 4), the structural damping must be known. Prior tests of these fan blades

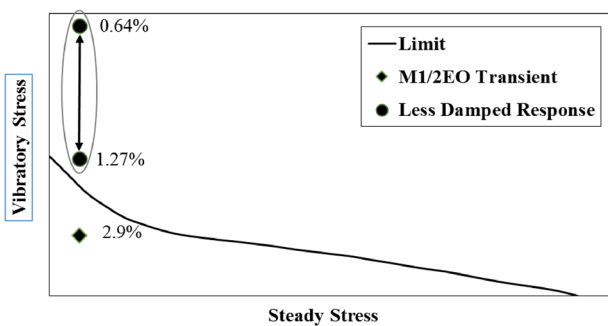


Fig. 13 Goodman diagram with a typical M1/2EO transient response point with high damping and region of more typical response from Ref. [13]

spun up in a vacuum spin rig showed that the structural damping was 0.002 (or 0.2%) for M1/2EO responses. Structural damping here is meant to include hysteretic material damping, blade root frictional damping, and any other vibration dissipation mechanism attributable to the test rig itself. It is possible that the nature of the distorted flow at half of design speed and reduced Mach number is such that it provides more aerodynamic damping than for a typical clean flow condition. This is a theory which should be researched in the future.

Due to the harmonic nature of the blade response as a result of the heavily distorted flow, there was concern pretest about the vibration amplitudes associated with this crossing. However, no analysis was run at this part speed condition to provide any concrete cause for alarm. But concern was abundant because of the strong second harmonic of the flow excitation evident in analysis performed at 85% and 100% speed [14,15]. Figure 13 shows that excursions up and down through the M1/2EO crossing were well below the Goodman limit. However, if the aerodynamic damping was more typical and in a range as presented previously, the amplitudes of vibration would have fallen in the region on Fig. 13 above the limit. Accumulation of cycles for mode 1 which are above this line may reduce the fan blade fatigue life. In the 8 × 6 wind tunnel testing, the fan accumulates less than 1000 cycles during these spool ups and shutdowns; however, in real operation on an aircraft upon landing, the fan may be spinning at a flight idle speed which could be close to this crossing. The response of the BLI blade here suddenly becomes a very important design consideration. It is evident that the design process for future fans intended to continuously ingest heavily distorted flows should include an analysis of fan response at a part speed condition such as flight idle.

Blade Response at Aerodynamic Design Point Conditions

The BLI²DTF fan never gets a break from distorted flow and its response is dominated by the synchronous and second harmonic

Table 4 Variation in frequency, amplitude, and damping for a typical M1/2EO response. Total Damping is also broken down into structural and aerodynamic components.

M1/2EO response at blade LE root gage

Blade SN	Speed (rpm)	Peak			Damping		
		Freq (hz)	Ampl (ksi pk)	Total (Zeta)	Structural	Aerodynamic	
1	5966	198.9	17.6	0.029	6.9%	93.1%	
2	5975	199.2	16.6	0.028	7.1%	92.9%	
9	5986	199.5	17.5	0.029	6.9%	93.1%	
17	6001	200.0	17.4	0.030	6.7%	93.3%	
21	5992	199.7	16.5	0.029	6.9%	93.1%	
22	5967	198.9	12.8	0.028	7.1%	92.9%	
Average	5981	199.4	16.4	0.029	6.9%	93.1%	

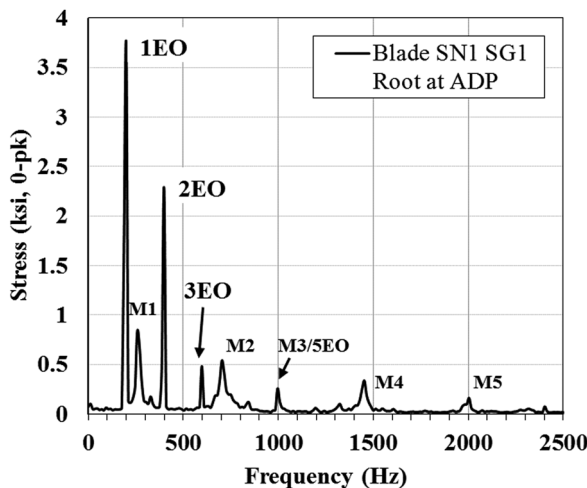


Fig. 14 Fast Fourier transform breakdown of blade 1 SG1 root vibration at ADP

components. Figures 14–17 show typical responses at each of the four gage locations at ADP. In all locations, the response is dominated by the 1EO component. The 2EO component too is larger in magnitude than almost all other blade frequency contributions. The 22.9% frequency margin between M1 and 1EO is clear in Fig. 14. Figure 16 shows the response near the tip of the blade. Peaks at the higher modes are apparent, but their amplitudes were small and well within limits. The blade responses at ADP as shown in Figs. 14–17 are well within stress guidelines established pretest, indicating that this fan could operate as its cruise condition for billions of cycles.

Comparison to Forced Response Analysis

Forced response analysis of the fan operating at ADP was performed as part of the blade design process. This analysis showed that the fan would respond to the primary once per revolution excitation and resulting harmonics imposed by the pressure distribution at the AIP shown in Fig. 4. Figures 18–20 provide a comparison of the NASA forced response blade vibration amplitudes at the first five engine orders to the actual gage stress values recorded during experiment. The analysis (for ADP) was done at a mechanical rotor speed of 11,864 rpm. The mechanical speed at ADP during 8×6 testing was usually around 12,050 rpm. All the responses presented so far are at this speed. For this comparison

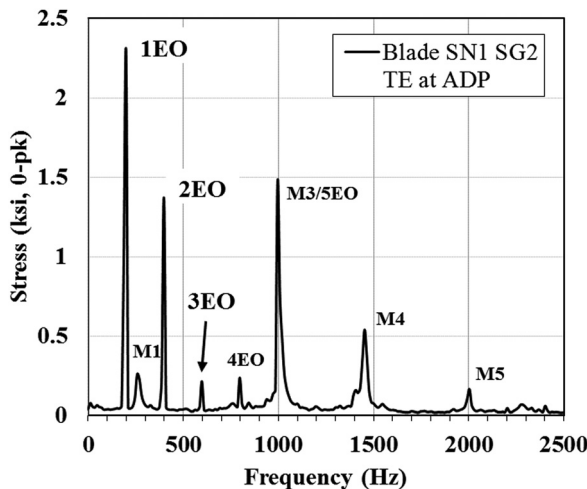


Fig. 15 Fast Fourier transform breakdown of Blade 1 SG2 TE vibration at ADP

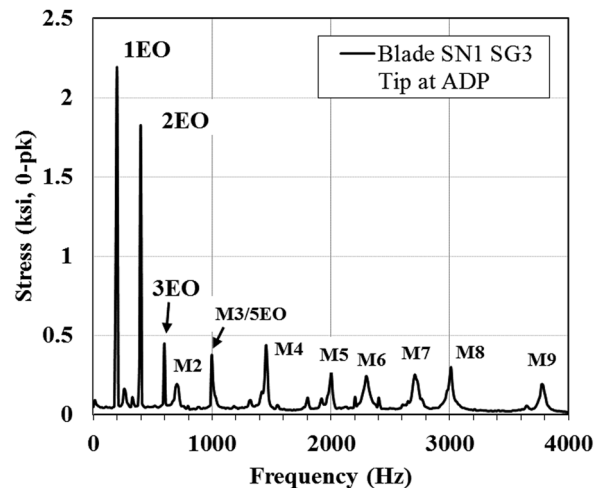


Fig. 16 Fast Fourier transform breakdown of blade 1 SG3 tip vibration at ADP

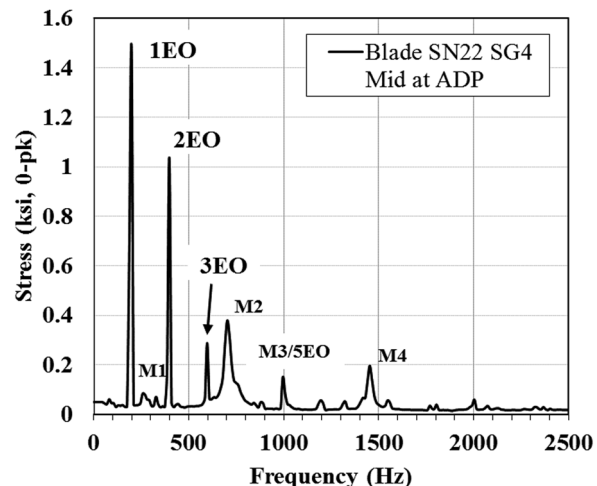


Fig. 17 Fast Fourier transform breakdown of blade SN22 SG4 Mid vibration at ADP

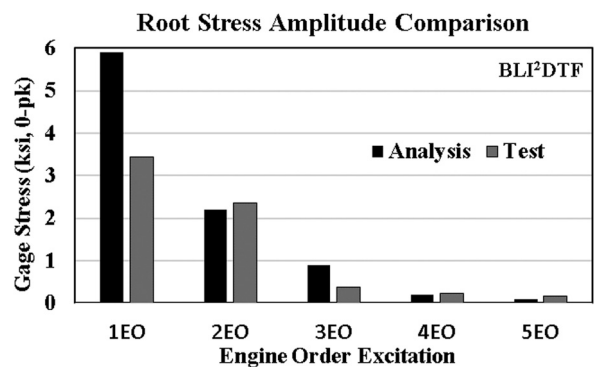


Fig. 18 Comparison of root gage (SG1) engine order response amplitudes

alone, however, blade engine order response amplitudes were extracted from test data at 11,849 rpm which was the closest obtainable result. Table 5 provides the amplitudes used in the comparisons shown in Figs. 18–20 as well as those of the blade resonances at 11,849 rpm. The trend in both analysis and the experiment at all gage locations is that 1EO dominates the

Table 5 Fast Fourier transform Amplitudes of select vibration frequency components at 11,849 rpm during wind tunnel testing near ADP

Mode/EO	SG1 (ksi)		SG2 (ksi)		SG3 (ksi)	
	Ave	Std Dev	Ave	Std Dev	Ave	Std Dev
1EO	3.44	0.36	1.72	0.72	2.00	0.37
M1	0.64	0.03	0.21	0.06	0.15	0.03
2EO	2.36	0.36	1.58	0.20	1.76	0.33
3EO	0.39	0.04	0.23	0.03	0.38	0.07
M2	0.59	0.03	—	—	0.21	0.04
4EO	0.24	0.06	0.25	0.08	0.15	0.08
5EO	0.16	0.05	0.69	0.17	0.27	0.08

response with 2EO less strong, but still notable. 3EO and 4EO magnitudes drop further and nearly fall into the levels of signal noise. The impact of 5EO varies depending on the sensitivity of the measurement location to mode 3. At the trailing edge, there is a strong response at 5EO. The mode 3 frequency is in close proximity (see Fig. 9) and is excited. The trailing edge gage location and orientation was selected for its sensitivity to mode 3 response (refer to Table 1). The amplitudes of EO responses depend significantly on their proximity to blade mode frequencies. The discrepancy between magnitudes in Figs. 18–20 may be attributable to small differences between the predicted and actual frequencies as shown in Fig. 9. One discrepancy unaccounted for is the large difference in the 1EO and 2EO responses at the blade tip. Also, it may be that the unsteady pressure distribution used in the forced response analysis did not accurately represent the true profile which the blades pass through at the tip. This may be because of the difference between the boundary conditions used in the computational fluid dynamic analysis and those in the 8×6 transonic tunnel section. But again, these blade gage response amplitudes are very low and well within gage stress limits.

Fan Flutter

Flutter of the BLI²DTF fan was seen once during testing while mapping the 100% speed line and searching for fan stall at Mach 0.78. The nonsynchronous flutter response was mode 1 at 266 Hz and had a nodal diameter of 2. At several speeds (including 100%), the variable area fan nozzle (VAFN) at the back of the rig was closed from its full open position in increments until either an instability was reached, or the nozzle reached its limit of travel. Figure 21 shows some preliminary fan mapping data for these speed line tests. This fan stage pressure ratio versus fan mass flow rate data shows that this fan has a significant stability margin. At 80% speed, the nozzle reached its travel limit before blade stall. At other higher speeds, blade stall was evident from the notable

Tip Gage Stress Amplitude Comparison

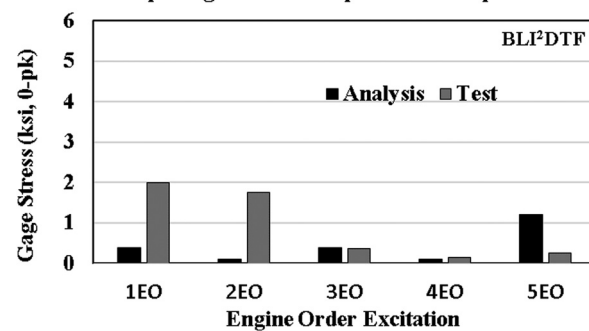


Fig. 20 Comparison of tip gage (SG3) engine order response amplitudes

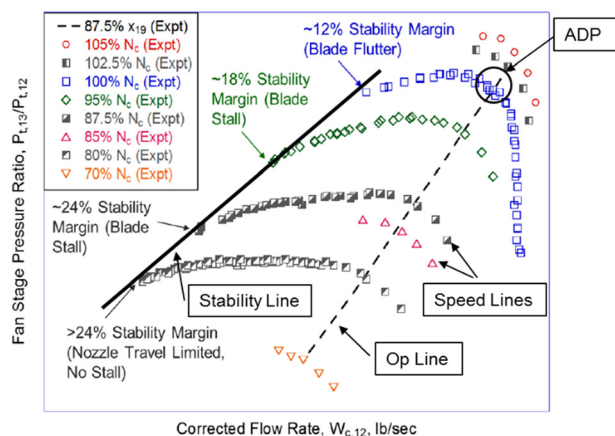


Fig. 21 Boundary layer ingestion propulsor preliminary fan map with fan stage pressure ratio plotted versus mass flow for qualitative reference

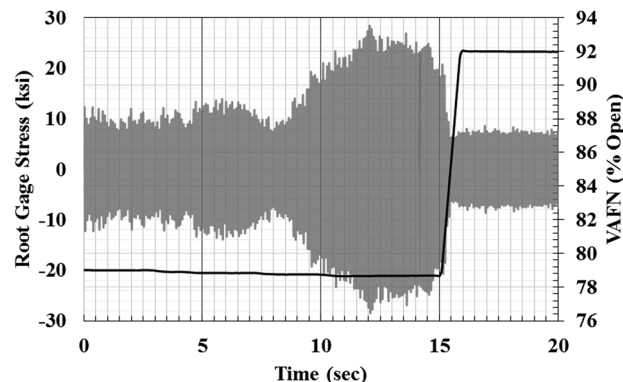


Fig. 22 Amplitude of blade SN17 root gage stress plotted with variable area nozzle position during flutter event

change in the dynamic pressure profile as measured by Kulites positioned just axially aft of the fan blade tip trailing edges.

At 100% speed, the fan fluttered before reaching stall. This occurred at a nozzle position of 78.7% open. Figure 22 shows the initiation and amplitude behavior of Mode 1 flutter as measured at the root of blade 17. Blade 17 was the high responder as shown in Fig. 23. The response shown before flutter is higher than usual as the nozzle was already closed to a position very close to 78.7% already. The fan was at the onset of flutter. The real-time position of the VAFN is also plotted with the response in Fig. 22. As the

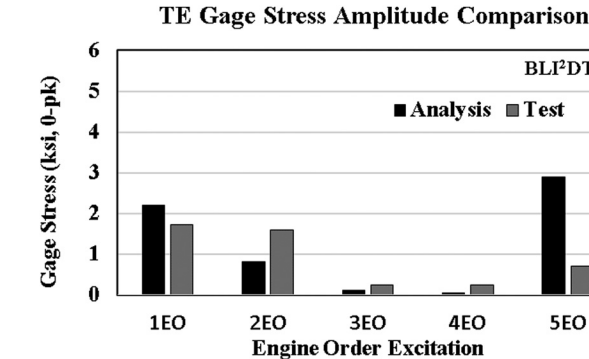


Fig. 19 Comparison of TE gage (SG2) engine order response amplitudes

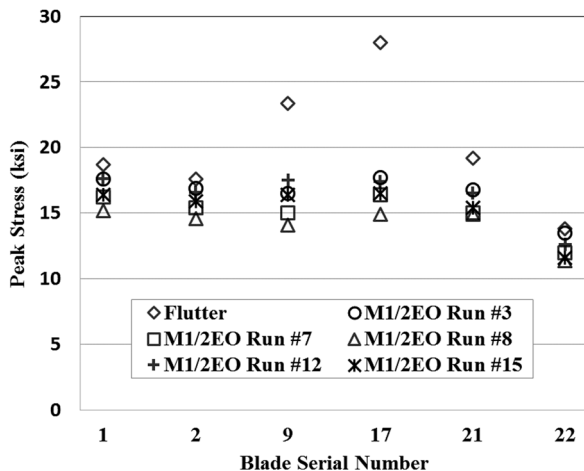


Fig. 23 A Comparison of blade dynamic stress at the root gage. Flutter event amplitudes and several M1/2EO crossing amplitudes shown.

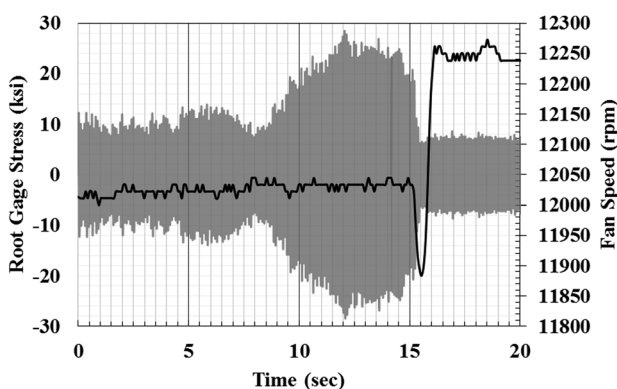


Fig. 24 Amplitude of blade SN17 Root gage stress plotted with fan speed during flutter event

VAFN was closed, the blades began to flutter at about 9 s. The amplitude increased until reaching a maximum at about 12 s. At 15 s, the VAFN was opened to the set safe position of 92%. The flutter dissipated rapidly as a result of the back pressure release. Figure 24 shows the same flutter response plotted along with the fan speed. When the VAFN began moving, the fan rubbed slightly which caused a reduction in speed. Once rubbing ceased, the fan accelerated to a speed slightly higher than ADP as the flow condition had changed and there was excess drive torque.

To put the flutter amplitudes into perspective, they are plotted on the Goodman Diagram along with the M1/2EO transient and the typical ADP root stress condition in Fig. 25. Some of the blade dynamic stress amplitudes are well above the limit.

Component Stress Versus Nozzle Position at Aerodynamic Design Point

Blade stresses changed with the back pressure on the fan which was controlled by the VAFN at the back of the test rig (see Fig. 2). Figures 26–29 show how each of the relevant response stress amplitudes changed with nozzle position along the 100% speed line (blue squares in Fig. 21). This section is included to show how the amplitudes of the stress components, mostly the first two engine orders and the first bending mode, change when the fan is running off of the operating line. The magnitude of the first two engine order responses of the blade do not change much along the op line of this fan. They do change with boundary layer thickness (BLT) (from 3.75–5.0 in). The 1EO and 2EO root component

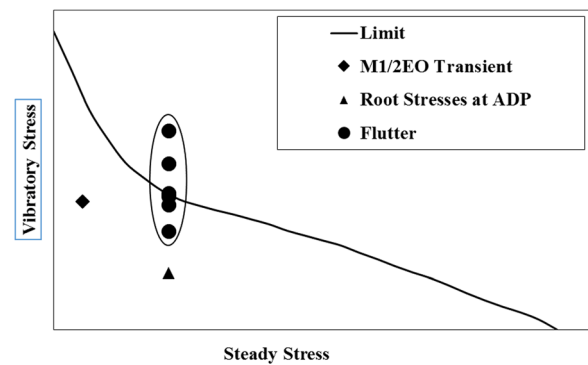


Fig. 25 Goodman diagram showing the mode 1 flutter gage stress amplitudes as they compare to other key mode 1 responses

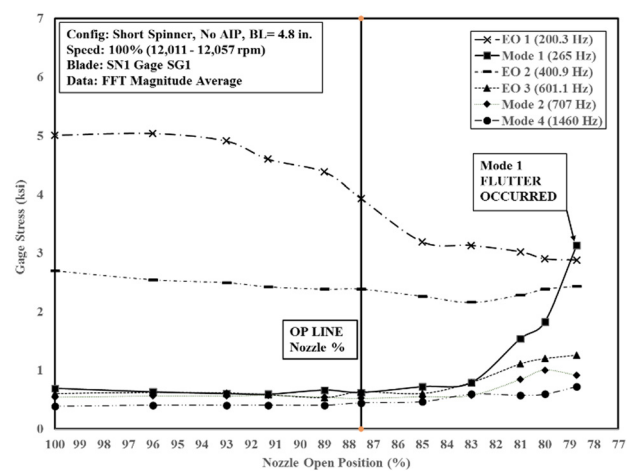


Fig. 26 Effect of nozzle position on gage stress for blade SN1 root gage (SG1) at ADP

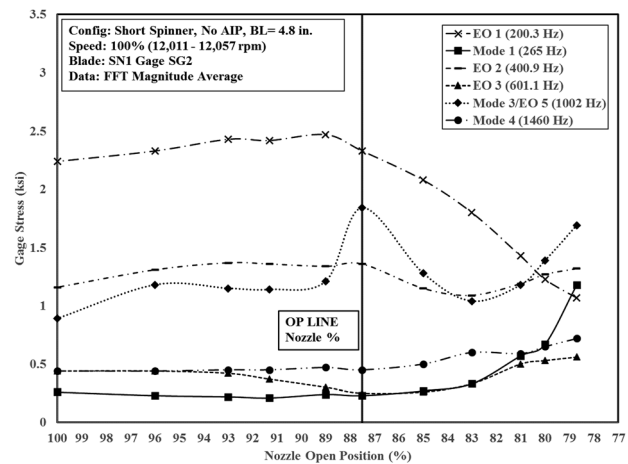


Fig. 27 Effect of nozzle position on gage stress for blade SN1 TE gage (SG2) at ADP

amplitudes at 5 in BLT reduce to 80% and 90% of their value at a BLT of 3.75 in. Details of these results are not presented herein however blade response results in this paper are shown for a BLT of 4.82 in.

Figure 26 shows the response at the root of the blade near the leading edge. The fan was at ADP and the nozzle was closed in

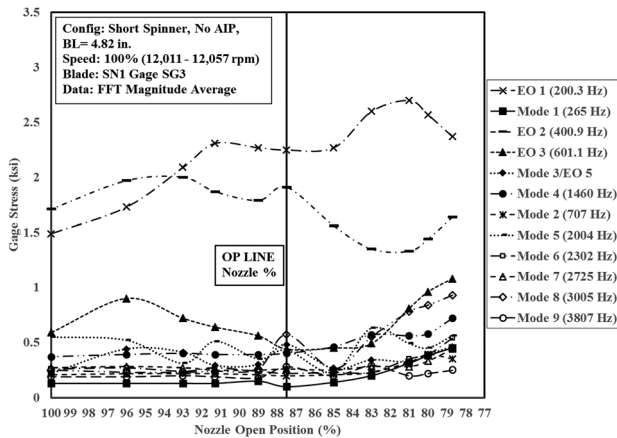


Fig. 28 Effect of nozzle position on gage stress for blade SN1 tip gage (SG3) at ADP

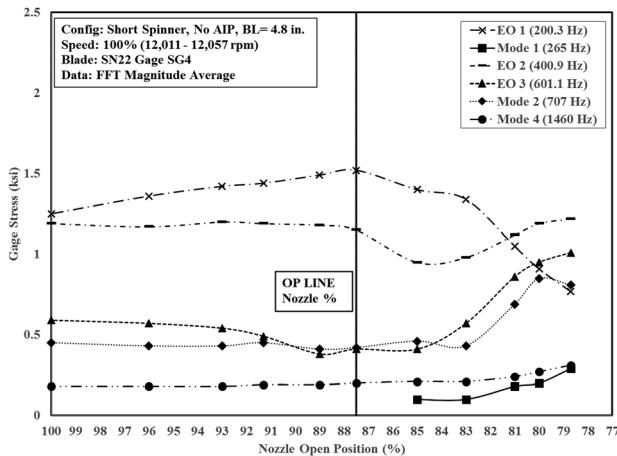


Fig. 29 Effect of nozzle position on gage stress for blade SN22 midblade gage (SG4) at ADP

incremental steps from 100% open to map out the 100% speed line. The 1EO and 2EO responses dominate the response until the blade approaches stall at 79% open nozzle. It can be seen that as the nozzle was closed from 83% to 78.7% the Mode 1 amplitude increased until flutter occurred. This was the only time the fan fluttered during testing. The 1EO response decreased as the nozzle was closed. The 2EO response decrease slightly until 83% then began to rise. With the nozzle open at 93% or higher, the 1EO component amplitude for this blade was 5 ksi peak. On the op line, the 1EO stress is 4 ksi peak. These stress amplitudes are well within the Goodman limit previously discussed.

Figure 27 shows the blade response at the trailing edge of the blade and approximately 1/3rd of span. Between 89 and 78%, the amplitude of Mode3 is cyclic. At ADP, the speed is just below the 5EOM3 crossing which occurs at 12,110 rpm. Though this Campbell crossing is not problematic, the response appears sensitive to changes in flow and pressure resulting from changes in nozzle position.

Figure 28 shows the response at the tip of the blade near the leading edge. The gage there picked up higher order blade modes in addition to the first 4 modes. Here too, the 1EO and 2EO frequencies dominate the overall blade response until flutter occurred.

To be complete, Fig. 29 shows the response at the middle of the blade. Here it is seen that the 1EO response decreases with decreasing nozzle position.

Conclusions

An integrated boundary layer ingesting inlet and distortion-tolerant fan was tested in the transonic section of the 8' × 6' Supersonic Wind Tunnel at the NASA Glenn Research Center. The fan blade design required several iterations and was analyzed by both UTRC and NASA Aeromechanics Engineers. Forced response and flutter analyses were performed and the fan design was deemed structurally sound to survive a wind tunnel test and to be aerodynamically stable in operation. The fan was mapped at Mach 0.78 and it survived the tests with no noticeable damage. The fan also proved to have a substantial stability margin without penalty associated with blade design modifications. The many changes in the final BLI²DTF blade design included a thicker root, a shorter tip chord, a restacking to balance moments around its center of gravity and modifications to accommodate surface shot peening. Currently, it is unknown as to the degree of significance of each of the changes made. It is desirable to understand the impact of every one of the changes to the reference blade which allowed the blade to accommodate the continuous distortion. Surely, the increase in the blade root thickness and the reduced chord length at the tip help move the M2/3EO crossing out of the operating range. But what price was paid in fan efficiency and can a thinner blade with a wider tip be designed to be robust in this application? Why wasn't the stability margin compromised by the changes? Certainly, there is more work to be done to understand this blade design and on how to keep fan engine order vibration component amplitudes and stability margins in check while upping the fan efficiency.

Frequencies for the first eight blade resonances determined through FEA were presented and matched to within 7% of actual at ADP and 105% speed. The predicted frequency margins at ADP and 105% speed matched well with those seen experimentally.

The most concerning response was the Mode 1 engine order 2 crossing (M1/2EO) during fan spool up and shutdown. The root stresses during these transients were close to the 10⁹ Goodman limit established for a titanium fan blade operating continuously in severe distortion. The 2.9% total damping of mode 1 during 2EO crossing seemed higher than is typical in clean flow. Hypothetical response amplitudes with traditional damping values of between 0.6 and 1.3% breach the Goodman limit which would likely reduce the fatigue lifespan of the blades. Forced response analysis was not done at this part speed M1/2EO condition, but for future blade designs, it might be appropriate to investigate it.

The fan fluttered while mapping the 100% speed line. The event lasted about 5 s and was thwarted by a rapid opening of the VAFN which caused the fan to lightly rub the case. Some of the gaged blade response amplitudes at flutter were over the Goodman limit.

Finally, the effect of VAFN position on blade vibration stress components was presented. In most cases, the 1EO and 2EO blade responses decreased as the nozzle was closed.

Acknowledgment

The authors are grateful to Dr. James Heidmann, the project manager of the AATT Project, and Chris Hughes, the BLI subproject manager, for their support of this work. The authors would also like to thank Mr. David Arend, the NASA Principal Investigator of the Boundary Layer Ingesting Inlet—Distortion-Tolerant Fan Task, for his steadfast diligence in making this a successful research project.

Nomenclature

AATT = Advanced Air Transport Technologies

ADP = aerodynamic design point

AIP = aerodynamic interface plane

BLI²DTF = boundary layer ingesting inlet/distortion-tolerant fan

DTF = distortion-tolerant fan

FFT = fast Fourier transform

LE = leading edge
 N = fan speed
 NASA = National Aeronautics and Space Administration
 NSMS = noncontacting stress measurement system
 P = pressure
 P_c = circumferential pressure
 P_t = total pressure
 TE = trailing edge
 UTRC = United Technologies Research Center
 VAFN = variable area fan nozzle
 W = weight flow rate
 x = axial position

References

- [1] Smith, L. H., 1993, "Wake Ingestion Propulsion Benefit," *AIAA J. Propul. Power*, 9(1), pp. 74-82.
- [2] Daggett, D., Kawai, R., and Friedman, D., 2003, "Blended Wing Body Systems Studies: Boundary Layer Ingestion Inlets With Active Flow Control," NASA Langley Research Center, Hampton, VA, Report No. [NASA/CR-2003-212670](#).
- [3] Kawai, R., Friedman, D., and Serrano, L., 2006, "Blended Wing Body (BWB) Boundary Layer Ingestion (BLI) Inlet Configuration and Systems Studies," NASA Langley Research Center, Hampton, VA, Report No. [NASA/CR-2006-214534](#).
- [4] Plas, A. P., 2007, "Performance of a Boundary Layer Ingesting (BLI) Propulsion System," *AIAA Paper No. 2007-450*.
- [5] Nickol, C. L., 2008, "Silent Aircraft Initiative Concept Risk Assessment," NASA Langley Research Center, Hampton, VA, Report No. [NASA/TM-2008-215112](#).
- [6] Nickol, C. L., and McCullers, L. A., 2009, "Hybrid Wing Body Configuration System Studies," *AIAA Paper No. 2009-931*.
- [7] Arend, D. J., Wolter, J. D., Hirt, S. M., Provenza, A. J., Gazzaniga, J. A., Cousins, W. T., Hardin, L. W., and Sharma, O. P., 2017, "Experimental Evaluation of an Embedded Boundary Layer Ingesting Propulsor for Highly Efficient Subsonic Cruise Aircraft," *AIAA Paper No. 2017-5041*.
- [8] Cousins, W. T., Voytovich, D., Tillman, G., and Gray, E., 2017, "Design of a Distortion-Tolerant Fan for a Boundary-Layer Ingesting Embedded Engine Application," *AIAA Paper No. 2017-5042*.
- [9] Hardin, L. W., Cousins, W. T., Wolter, J. D., Arend, D. J., and Hirt, S. M., 2018, "Data Analysis Techniques for Fan Performance in Highly-Distorted Flows From Boundary Layer Ingesting Inlets," *AIAA Paper No. 2018-1888*.
- [10] Duffy, K. P., Provenza, A. J., Bakhele, M. A., Min, J. B., and Abdul-Aziz, A., 2018, "Laser Displacement Measurements of Fan Blades in Resonance and Flutter During the Boundary Layer Ingesting Inlet and Distortion-Tolerant Fan Test," *AIAA Paper No. 2018-1892*.
- [11] Bakhele, M. A., Reddy, T. S., Coroneos, R. M., Min, J. B., Provenza, A. J., Duffy, K. P., Steffko, G. L., and Heinlein, G., 2018, "Aeromechanics Analysis of a Distortion-Tolerant Fan With Boundary Layer Ingestion," *AIAA Paper No. 2018-1891*.
- [12] Min, J. B., Reddy, T. S., Bakhele, M. A., Coroneos, R. M., Steffko, G. L., Provenza, A. J., and Duffy, K. P., 2018, "Cyclic Symmetry Finite Element Forced Response Analysis of a Distortion Tolerant Fan With Boundary Layer Ingestion," *AIAA Paper No. 2018-1890*.
- [13] Cardinale, V. M., Bankhead, H. R., and McKay, R. A., 1980, "Experimental Verification of Turbuloblading Aeromechanics," Turbine Engine Testing AGARD Conference, Session IV Complete Powerplant Testing, Part I, p. 23.
- [14] Bakhele, M. A., Reddy, T. S., Herrick, G. P., Shabbir, A., and Florea, R. V., 2012, "Aeromechanics Analysis of a Boundary Layer Ingesting Fan," *AIAA Paper No. 2012-3995*.
- [15] Bakhele, M. A., Reddy, T. S., and Coroneos, R. M., 2014, "Forced Response Analysis of a Fan With Boundary Layer Inlet Distortion," *AIAA Paper No. 2014-3734*.